IOPscience iopscience.iop.org

Home Search Collections Journals About Contact us My IOPscience

Stretchable electronics: materials, architectures and integrations

This article has been downloaded from IOPscience. Please scroll down to see the full text article.

2012 J. Phys. D: Appl. Phys. 45 103001

(http://iopscience.iop.org/0022-3727/45/10/103001)

View the table of contents for this issue, or go to the journal homepage for more

Download details:
IP Address: 115.145.165.11
The article was downloaded on 09/03/2012 at 06:51

Please note that terms and conditions apply.

J. Phys. D: Appl. Phys. **45** (2012) 103001 (14pp) doi:10.1088/0022-3727/45/10/103001

TOPICAL REVIEW

Stretchable electronics: materials, architectures and integrations

Jong-Hyun Ahn[1] **and Jung Ho Je**[2]

[1] School of Advanced Materials Science and Engineering, SKKU Advanced Institute of Nanotechnology, Sungkyunkwan University, Suwon 440-746, Korea
[2] X-ray Imaging Center, Department of Materials Science and Engineering, Pohang University of Science and Technology, Pohang 790-784, Korea

E-mail: ahnj@skku.edu and jhje@postech.ac.kr

Received 8 December 2011, in final form 30 January 2012
Published 22 February 2012
Online at stacks.iop.org/JPhysD/45/103001

Abstract
Stretchable electronics, i.e. elastic electronics that can be bent and stretched, is a new, emerging class of electronics, based on building electronic circuits or devices on stretchable substrates. The potential applications range from fully conformable, stretchable, skin sensors for robotic devices, wearable electronic devices, to flesh-like biodevices. One of the challenges in the development of stretchable electronics is to retain full functionality under high external strains in stretching. In this paper, we review a few approaches recently developed for stretchable electronics and highlight recent research efforts on multi-directional writing for stretchable, three-dimensional structures.

(Some figures may appear in colour only in the online journal)

1. Introduction

Stretchable electronics have attracted a great deal of attention because of their potential applications in various areas ranging from robotic sensory skins and wearable communication devices to bio-integrated devices [1, 2]. One of the most difficult challenges in the development of stretchable electronics is the simultaneous achievement of both excellent mechanical robustness and electronic performance. Specifically, constituent materials and devices in stretchable integrated systems must be designed so that their mechanical and electrical functionality are preserved under high strain values.

In recent years, stretchable electronics have been mostly studied in two different strategies. The first is 'wavy structural configuration' methods that use rigid semiconductor nanowires, nanoribbons and nanomembranes configured into 'wavy' shapes, which can accommodate large applied strains without fracturing the materials [3–5]. This approach relies on nonlinear buckling phenomena, well known in systems comprised of a thin stiff layer on a soft substrate. When a rigid thin film bonded to an elastomeric polymer substrate is subjected to compressive stress, the film relieves the surface strain by mechanical buckling. External strains in stretching can then be accommodated by relaxing the pre-strain and changing the buckles' wavelengths and amplitudes, thereby improving the stretchability significantly in active devices and/or passive interconnects. As another type of wavy configuration, 2D horseshoe metal or three-dimensional (3D) metal interconnects can effectively sustain maximum ($>100\%$) elongation [6, 7].

The second strategy is 'stretchable interconnects' methods that use stretchable electrodes to interconnect rigid active device islands on elastomeric substrates [8]. The fundamental process for stretchable interconnects is to blend highly conductive materials with soft elastic materials such as rubber-like elastomers. This approach is attractive because conventional, high-performance electronic components can be implemented on soft substrates by well-known processes. For stretchable composite interconnects, a variety of highly conductive materials such as metal wires, conducting polymer, carbon nanotube or graphene films have been applied [9–13]. Stretchable interconnects were then produced on elastic substrates by various processes including vacuum evaporation,

 © 2012 IOP Publishing Ltd Printed in the UK & the USA

photolithographic patterning, transfer printing and screen printing [14–19]. This approach is, however, limited to two-dimensional (2D) structure and low aspect ratio features that should be supported by substrates.

Omnidirectional and individual integration in stretchable electronics remains as a challenge in the above two strategies. As an alternative approach to overcome the challenge, 'multi-directional writing' of highly conductive organic or inorganic materials onto elastic substrates at relatively low temperatures has been explored very recently [20]. This approach offers not only high stretchability but also accurately controlled shapes and positioning of each stretchable 3D structure. Indeed multi-directional writing has been successfully demonstrated in stretchable device arrays and circuits on elastomeric substrates in 2D and 3D layouts [20].

In this paper, we review the aspects of stretchable active electronic components and passive interconnects, and their integration into stretchable electronic devices. The content begins with classes of materials and architectures for high-performance stretchable electronics. Next we focus on multi-directional writing for highly conductive organic or inorganic materials onto elastic substrates. Then, representative examples of devices and integrated systems in either 2D or 3D layouts will be presented in the last section.

2. Classes of materials and architectures for stretchable electronics

Till now two main classes of materials are frequently used for electrodes in electronic devices; one is well-known inorganic metals (Al, Au, Mo, Ti, Ag) and metal oxide (ITO), and the other is organic conductive polymers such as PEDOT : PSS. The realization of flexible, stretchable devices using conventional metal or semiconducting materials is difficult because they sustain very small strain value (<1%), compared with elastomeric substrates. The strain sustainability (<5%) of conductive polymers, despite being much better than metals, is not enough for stretchable electronics as well. Moreover, conducting polymers have an ageing problem, degrading with time.

Presently, researchers are engaged in search of flexible, stretchable and conductive materials by employing two main approaches: 'wavy structural configuration' and 'stretchable interconnects' methods, as mentioned above. Details of these two approaches will be first summarized here. 'Multi-directional writing' approach of highly conductive organic or inorganic materials onto elastic substrates will be described in the next section.

2.1. Wavy structural configuration

In this section, we review two representative approaches of wavy structures for stretchable electronics; (1) mechanical buckling and (2) 2D or 3D configuration of metal interconnects.

2.1.1. Mechanical buckling for stretchable 'wavy' structures. Mechanical buckling method is a promising approach to realize stretchable 'wavy' structures on elastomeric substrates [21–24]. This approach makes brittle inorganic materials flexible and stretchable.

As schematically illustrated in figure 1(*a*) [1], the fabrication process of silicon (Si) wavy buckles involves three steps: (i) fabrication of thin Si ribbons on an Si wafer by conventional lithographic process, (ii) bonding the ribbons to a pre-strained elastomeric substrate (polydimethylsiloxane, PDMS) and (iii) peeling back the PDMS bonded with the ribbons from the Si wafer, then releasing the pre-strain immediately. This relaxation leads to the spontaneous formation of well-controlled, highly periodic, wavy structures in the ribbons, as demonstrated in the SEM image of figure 1(*b*). Interestingly, these wavy structures can be not only flexed but also stretched and compressed, similar to an accordion bellows. Figure 1(*c*) shows Si p–n diode ribbons stretched and compressed well in the range of 11%.

This buckling approach can expand its application scope to various nanomaterials, as seen in buckled Si nanowires (figure 1(*d*)) [25] and buckled single-walled carbon nanotubes (SWNTs) (figure 1(*e*)). Stretchability of Si nanowires was reported to increase up to 100% by controlled bucking. The molecular scale (∼1 nm) buckled SWNTs in figure 1(*e*) can be applied for mechanically stretchable nano-electronic devices [26]. In addition to the buckling approach, the conformal fabrication of stiff thin films on compliant substrates with sinusoidal, 'wavy' features of surface relief represents an alternative method that can avoid any initial film strain and as a result, achieve high stretchability [27].

2.1.2. 2D or 3D configuration of metal interconnects. We first discuss horseshoe configuration for stretchable metal interconnects. A simulation was carried out to obtain a horseshoe shape for a stretchable interconnect between two islands [28–30]. Horseshoe metal interconnects were practically formed by joining a series of circular arcs, as shown in the top of figure 2(*a*). The stress sustainability in these horseshoe interconnects was governed by three parameters: the angle between the horizontal line and the extremity of the shape (H), the width (w) and the diameter (D). In these particular horseshoe shapes, most of the stresses were accommodated in the wider region whereas the smaller zone had negligible stress. Specifically, a high maximum elongation was sustained with a high electrical resistance at H_{45} whereas a low elongation with a low electrical resistance at H_0. The pitch was reduced drastically at a stackable structure of H_{20} [31, 32]. According to the required application, metal interconnects could be designed with a compromise between the high maximal elongation and the low track resistance. Figure 2(*a*), bottom, shows prototype high-frequency stretchable interconnects.

In addition to the 2D horseshoe interconnects in figure 2(*a*), 3D configurations of metal interconnects have also been tried, in particular, using electroplating or electroless deposition [33–36], microcasting [37, 38], LIGA (lithographie, galvanoformung, und abformung) and solder reflow [39, 40]. The 3D fabrication, however, is still very limited, not applicable for general purpose. For instance, electrodeposition or electroplating technique requires multiple

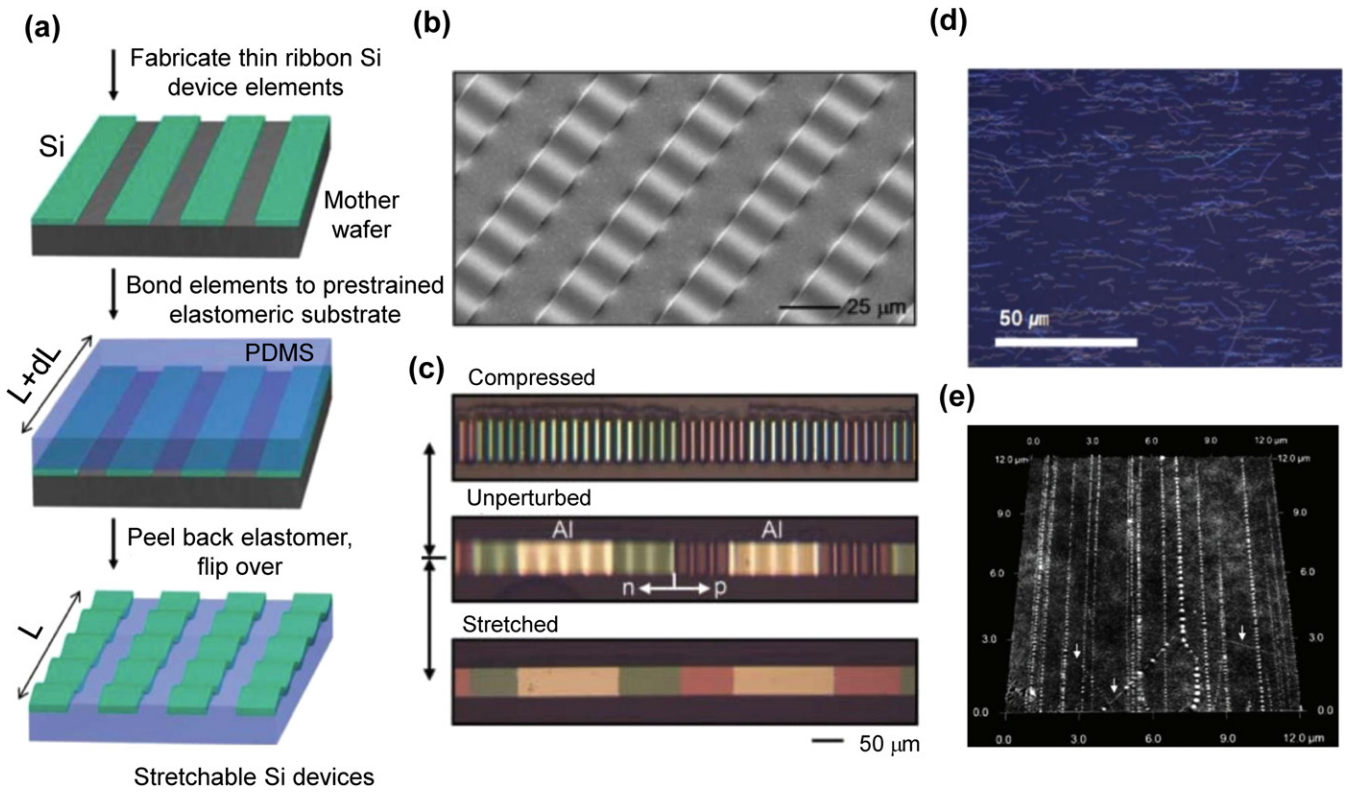

Figure 1. Mechanical buckling for wavy configuration. (*a*) Schematic illustration of the buckling process for building stretchable Si devices on elastic substrates. (i) Fabrication of thin Si ribbons by a conventional lithographic process; (ii) bonding the ribbons to a pre-strained elastomeric substrate (PDMS); (iii) wavy ribbon structures induced by the relaxation of the pre-strain. (*b*) SEM image of wavy Si ribbons with uniform wavelengths and amplitudes. (*c*) Stretching test of wavy Si p–n diode ribbons on a PDMS substrate −11% (top), 0% (middle), and 11% (bottom). From [21]. Reprinted with permission from AAAS. (*d*) Optical micrograph of buckled Si Nanowires. Reprinted with permission from [25]. Copyright 2009 American Chemical Society. (*e*) AFM image of molecular scale buckled SWNTs. Reprinted with permission from [26]. Copyright 2008 American Chemical Society.

lithography steps of layer-by-layer patterning, implying a very slow and costly process.

For 3D metal interconnects, Siegel *et al* [41] developed a microsolidics method by injecting a liquid metal solder into microfluidic channels and cooling it. The fabrication process consisted of five steps: (1) fabrication of microfluidic channels in PDMS, (2) plasma oxidation and silanization of the channel inner surfaces for wetting, (3) introducing the solder into the channels, (4) cooling the channels for solidification, and (5) bending, twisting, rolling or deforming the system into desired shapes, depending on the applications. Indeed metallic wires could be designed to any desired shape, as wrapped around a capillary tube or tied into a knot in figure 2(*b*), left or right. Interestingly, if the metal interconnects are accidentally broken during elongation, the defective parts can be repaired simply by heating the interconnects to molten states and then sonicating them to reconnect the broken parts inside the channels.

Another approach of 3D metal interconnects based on noncoplanar mesh design was also proposed for stretchable electronics [7, 42]. As seen in figure 2(*c*), an array of CMOS inverters with noncoplanar mesh of serpentine bridges was integrated on an elastomeric substrate. When the devices were subjected to an external strain along the x or y direction, the noncoplanar serpentine bridges effectively compensated the applied strain by changing the height as well as the geometry of serpentine shape. As shown in the optical image of figure 2(*c*), the CMOS inverter array was sustainable under stretching test up to 70% along the x and y directions. A maximum stretchability up to ∼140% was successfully demonstrated without fracturing in this configuration.

2.2. *Stretchable interconnects by conducting material/elastomer composites*

For the fabrication of stretchable composite interconnects, various kinds of conducting materials such as conductive polymers, carbon nanotubes and graphene are embedded in soft elastic materials, as will be described below in detail.

2.2.1. Conductive polymer/elastomer composites. The interconnection networks should be basically elastic with their high performance in developing elastic electronics that undergoes stretching as well as bending. Initially, interconnects were made by embedding metal particles in an elastomer such as silicone [43, 44]. The problem in this approach is limited mechanical properties; electrical conductivity significantly changes with strain. As an alternative, conductive polymer/elastomer composites have been explored. One advantage of these materials as stretchable electrodes is their excellent printability and stretchability. A typical fabrication method of composites is based on impregnating conducting polymer fibres [45–47] into

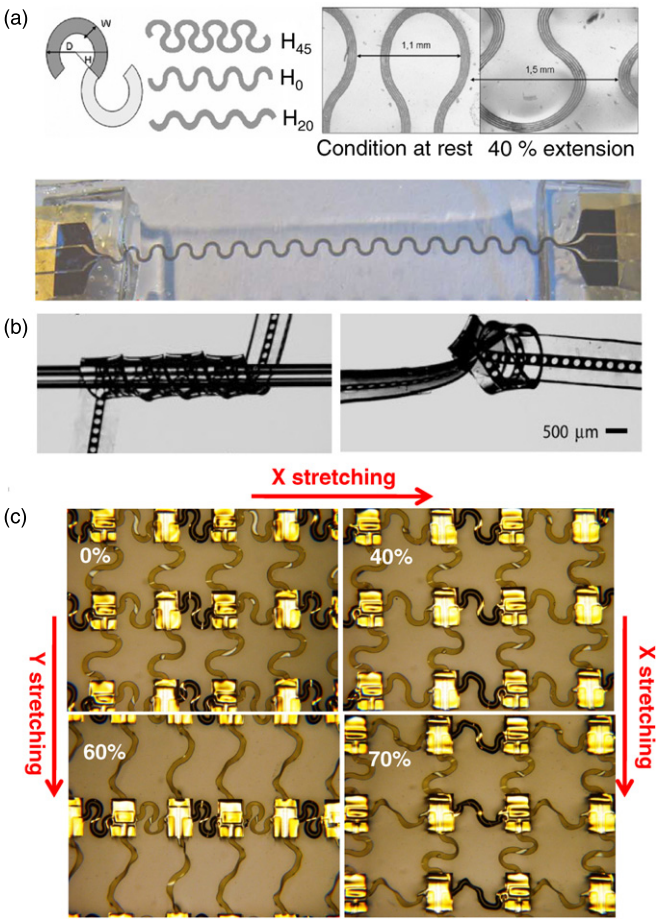

Figure 2. (*a*) Top images show the schematic representation of horseshoe-shaped stretchable interconnects. Bottom photograph shows the prototype stretchable high-frequency interconnects. (*b*) Images of flexible metallic wires embedded in PDMS wrapped around a glass capillary (left) and tied into a knot (right). From [33]. Reprinted with permission from AAAS. (*c*) Optical images of stretching test in noncoplanar electronics with serpentine bridges.

polyurethane foam [48–50]. The main obstacle in applying the composite materials to stretchable electronics is their low conductivities, usually below 1 S cm^{-1}.

Hansen *et al* [51] significantly improved the conductivity by developing a highly elastic and stretchable conductive polymeric material, specifically by blending poly(3,4-ethylenedioxythiophene) : p-tosylate (PEDOT) and polyurethane elastomer (PUR). The polymer blend solution, obtained by spin coating, could be printed in stretchable electronics. The conductivity reached to 100 S cm^{-1} even under stretching more than 100%.

The four-point method for measuring the conductivity of as-prepared PEDOT/PUR blend films using four copper wires separated by 10 mm is shown schematically in figure 3(*a*). Figure 3(*b*) demonstrates the variation of relative resistance/conductivity as a function of the elongation numbers for three different samples with 33, 40 and 50 wt% of PEDOT. The resistance, which was monitored when stretched up to 50% and relaxed to 0% for the 10 cycles, showed stable and reversible behaviour except for the irreversible increase in initial elongation. The developed resistance for initial elongations was still lower as it would be expected for metallic

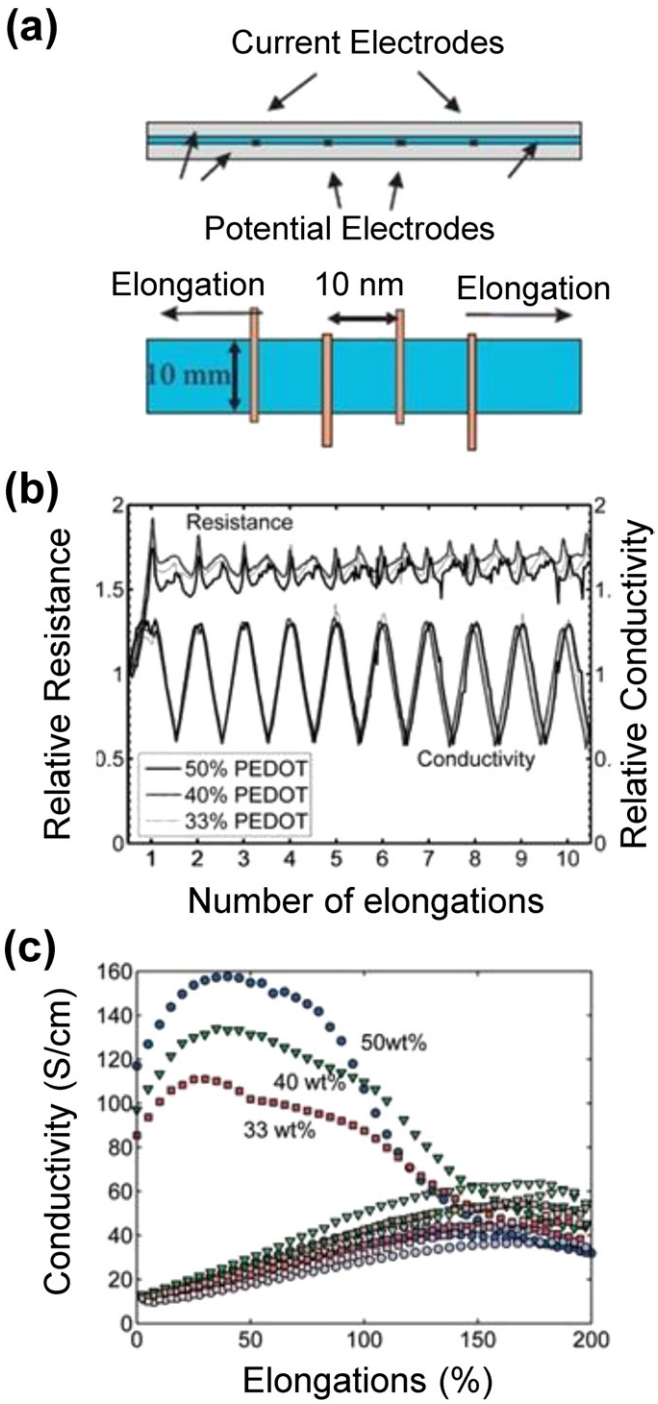

Figure 3. (*a*) Schematics of four-point resistance measuring set-up for the PEDOT/PUR/PEDOT sandwiched film, (*b*) relative resistance and conductivity for 50, 40 and 33 wt% of PEDOT with respect to cyclic elongation (10 times) subjected to 50% strain, (*c*) conductivity versus elongation of the 50% PEDOT (circles), 40% PEDOT (triangles) and 33% PEDOT (squares) during repeated straining by 200%. From [51]. Reprinted with permission from Wiley.

materials. Figure 3(*c*) shows the conductivity variation of another similar set of films as a function of strain up to 200% for the two cycles. The conductivity increased in the initial stages but decreased in the later stages for all three samples (33, 40 and 50 wt%). The 40% PEDOT/PUR blend sample showed the highest conductivity over ∼90–100% strain. The

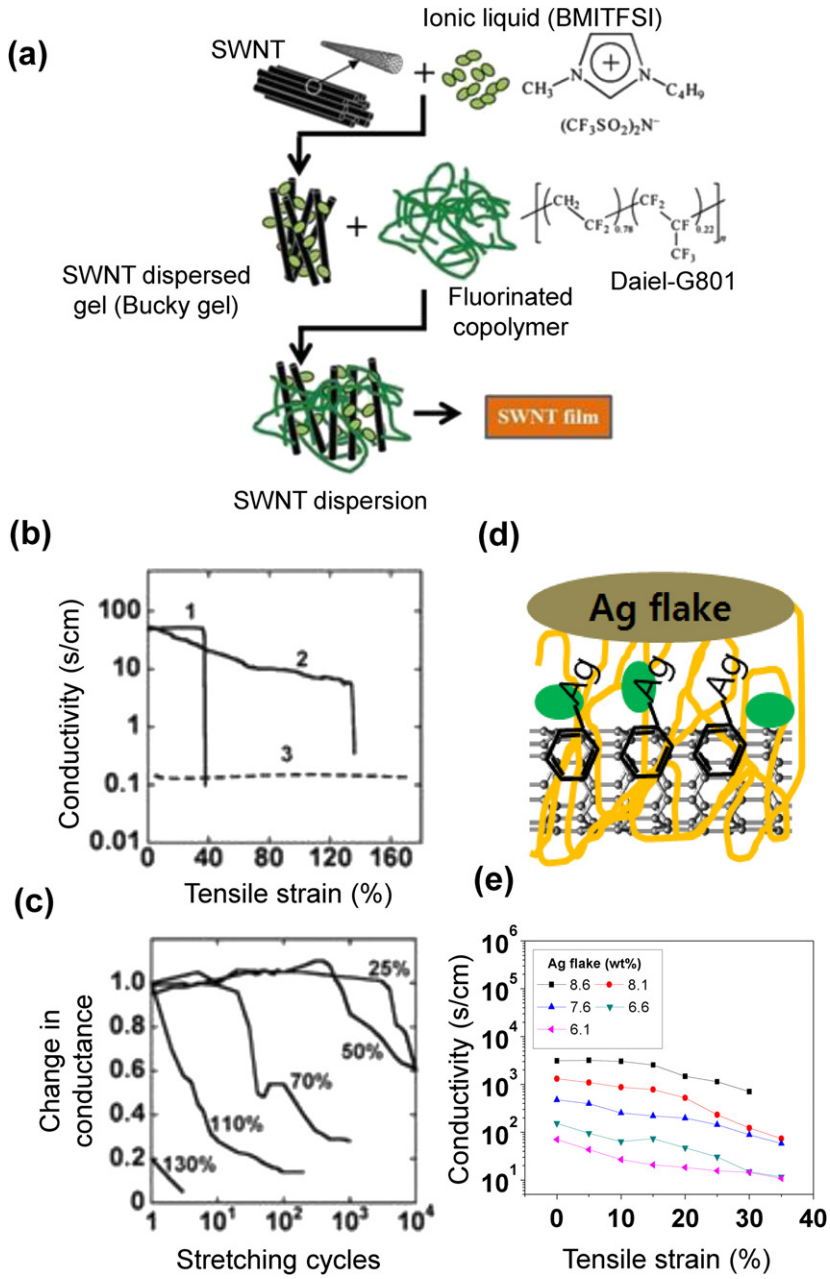

Figure 4. (*a*) Schematic representation of the synthesis procedure for SWNT film, SWNT elastic conductor and SWNT paste, (*b*) conductivity with respect to uniaxial strain for SWNT film (1), SWNT elastic conductor (2) and commercially available carbon-particle-based elastic conductor (3), (*c*) variation in conductance of SWNT elastic conductor under uniaxial stretching (25%, 50%, 70%, 110% and 130%) cycles. From [53]. Reprinted with permission from AAAS. (*d*) Schematic representation of hybrid Ag–MWNT composite film, (*e*) conductivity variation with respect to tensile strain for five different wt% of Ag flakes in hybrid Ag–MWNT composite film; inset shows the cycling test under 20% tensile strain. Reprinted by permission from Macmillan Publishers Ltd: [54], copyright 2010.

resistance behaviour was similar and showed reproducibility for the entire samples, as seen in figure 3(*b*). All the samples showed substantial conductivity of ∼10–50 S cm^{-1}, even at 200% strain.

2.2.2. SWNT/elastomer composites. Much effort has been made by many researchers towards carbon nanotubes/polymer composite electrodes in rubber-like stretchable electronics. The conductivity obtained, however, was still low typically, ∼10^{-3}–10^{1} S cm^{-1} [52]. For instance, Sekitani *et al* [53] developed a transistor-active matrix to fabricate SWNT composite films with a biaxial stretchability up to 70%. A highly elastic conducting gel was produced by dispersing millimetre-long SWNTs, acting as stable chemical dopant, in vinylidene fluoride–hexafluropropylene copolymer matrix with the help of an ionic liquid 1-butyl-3-methylimidazolium bis(trifuromethanesulfonyl)imide, as illustrated in figure 4(*a*). The conductivity of the SWNT composite film obtained from the gel was as high as 10 S cm^{-1}, despite being decreased by the extraction of the ionic liquid.

The elasticity improvement of SWNTs film was achieved by composing the SWNTs film with PDMS, Sylgard 184. The resulting composite film was referred to as an elastic conductor.

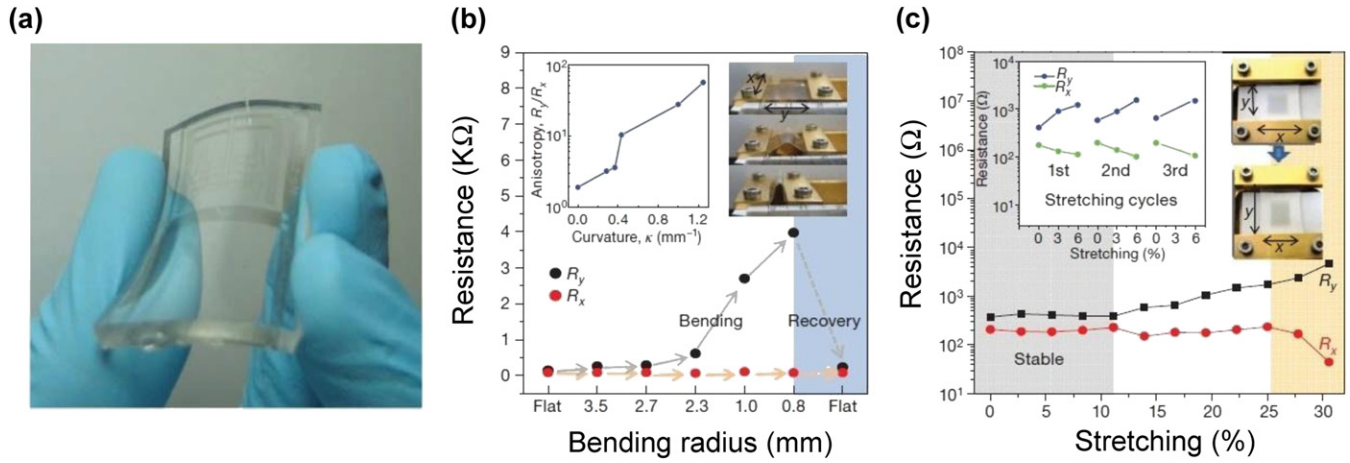

Figure 5. (*a*) Photograph of transparent and flexible graphene films transferred on PDMS substrate, (*b*) variation in resistance of a graphene film transferred to a 0.3 mm-thick PDMS/PET substrate for different distances between holding stages (that is, for different bending radii). The left inset shows the anisotropy in four-probe resistance, measured as the ratio, R_y/R_x, of the resistances parallel and perpendicular to the bending direction, y. The right inset shows the bending process. (*c*) Resistance of a graphene film transferred to a PDMS substrate isotropically stretched by 12%. The left inset shows the case in which the graphene film is transferred to an unstretched PDMS substrate. The right inset shows the movement of holding stages and the consequent change in shape of the graphene film. Reprinted by permission from Macmillan Publishers Ltd: [13] copyright 2009.

Figure 4(*b*) shows the conductivity variation as a function of tensile strain for (1) a SWNT film, (2) the SWNT elastic conductor and (3) a commercially available conducting rubber containing carbon particles as a reference. The SWNT film maintained its excellent high conductivity of ∼57 S cm^{-1} up to 38%, but immediately dropped afterwards. In comparison, the conductivity of the SWNT elastic conductor, even if gradually decreased from the initial high conductivity of 57 S cm^{-1}, showed a large strain sustainability of 138% with a conductivity value of ∼6 S cm^{-1}, which was much larger than that of the commercially available conducting rubber. The SWNT elastic conductors showed degradations in conductivity with stretching cycles, specifically, larger degradations at higher strains, as demonstrated in figure 4(*c*). In spite of irreversible conductance changes at such large strains beyond 110%, the conductivity was still higher than 1 S cm^{-1}.

Recently, Chun *et al* [54] reported highly conductive, printable and stretchable hybrid composite materials by combining micrometre-sized silver flakes and multiwalled carbon nanotubes (MWNTs) decorated with self-assembled silver nanoparticles (nAg). The carbon nanotubes here worked as an effective electrical network among the silver flakes. An Ag–MWNT composite film was formed by the conjugation of Ag nanoparticles and MWNTs by means of π–π interaction (figure 4(*d*) [55–58]. By mixing the nAg–MWNTs in 1-butyl-4-methylpyridinium tetrafluroborate and pyridinium-based ionic liquid, a nAg–MWNT conducting gel was prepared and then mixed with silver flakes, followed by a sonication in a copolymer polyvinylidenefluoride (PVDF) solution. Finally, the hybrid Ag–MWNT composite film (thickness ∼140 μm) was prepared by drop casting, drying and curing at 160 °C. Figure 4(*e*) shows the conductivity behaviour of the hybrid nAg–MWNT composite films for different Ag flake concentrations. Even though the conductivity decreased with tensile strain, a high conductivity of 706 S cm^{-1} was obtained at a strain of 30% for an Ag flake concentration of 8.60 wt%. The stretchability was rarely affected by the Ag flake concentration. All the films ruptured at ∼35% tensile strain. Repeatability test up to 5000 cycles shows that the conductivity was very stable except for the initial decrease, reaching a value of 1510 S cm^{-1}.

2.2.3. Graphene: transparent conductive film. Graphene has attracted considerable attention for its use as an electrode in stretchable electronics due to the high conductivity and excellent stretchability. Recently Kim and Bae *et al* [13] and Bae *et al* [59] have developed a direct growth method of large-scale graphene films using chemical vapour deposition on thin nickel or copper layers as well as two other transferring methods on arbitrary substrates. The transferred graphene films showed a very low sheet resistance of ∼30 Ω/square with 90% optical transparency. The electron mobility for the transferred graphene films to the silicon dioxide substrate was greater than 3700 cm^2 V^{-1} s^{-1}. Figure 5(*a*) shows high transparency and high flexibility in a graphene film transferred to a PDMS substrate. For graphene films transferred on a polyethylene terephthalate (PET) substrate (thickness ∼100 μm) coated with a thin PDMS layer (thickness ∼200 μm), the resistances showed little change with bending radii up to 2.3 mm, steeply increasing afterwards (figure 5(*b*)). The resistance, however, was completely recovered on unbending, indicating the good foldability of previously reported graphene films [60]. Figure 5(*c*) exhibits the resistance behaviour of graphene films transferred to an unstrained (inset) and a pre-strained PDMS substrate with respect to uniaxial tensile strain ranging from 0% to 30%. The resistance was recovered to its original value after stretching by ∼6% for the graphene films on the unstrained substrate, showing a mechanical failure beyond ∼6%. The stretchability was significantly improved for the graphene films transferred on the isotropically pre-strained (∼12%) PDMS substrate. Specifically, the stretchability improved to ∼11% with little

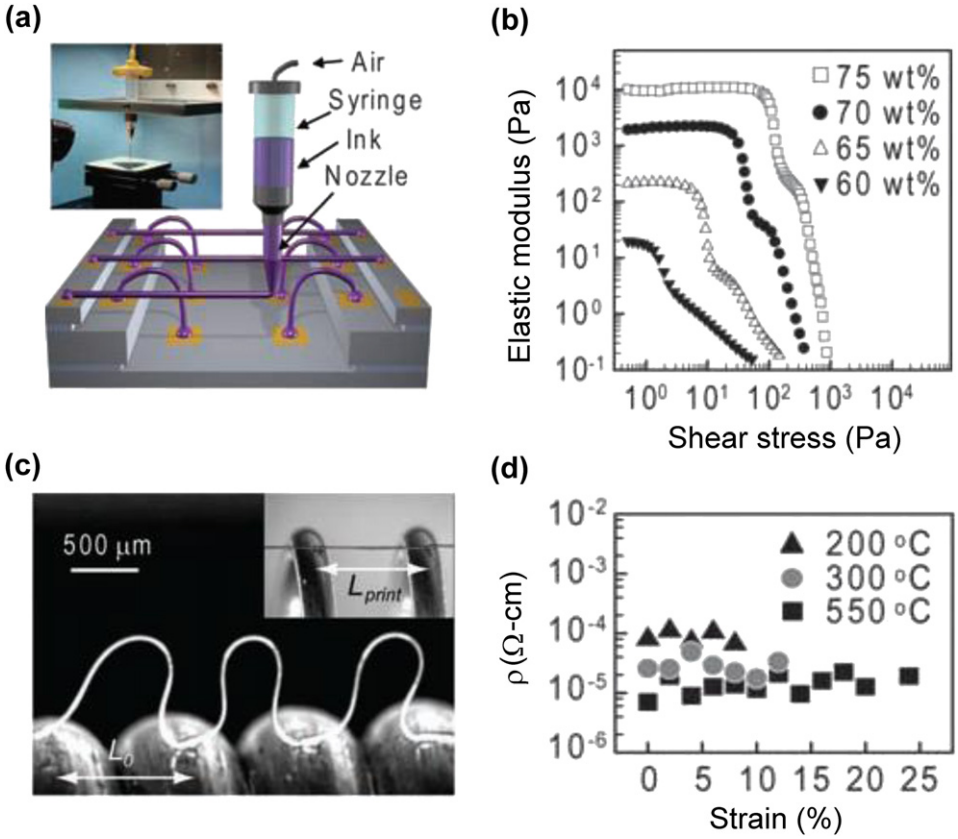

Figure 6. Direct ink writing for stretchable microelectrodes. (*a*) Schematic illustration showing multi-directional printing of stretchable silver microelectrodes by the direct ink writing method and optical image of apparatus used (inset), (*b*) shear elastic modulus versus shear stress for silver nanoparticle inks of varying solid loading, (*c*) optical image showing stretchable silver microarches integrated onto a spring, (*d*) electrical resistivity of silver microarches versus strain and annealing temperature. From [20]. Reprinted with permission from AAAS.

change in the longitudinal and transverse resistances and up to ∼25%, sacrificing the resistances, in particular, R_x, by one order of magnitude, indicating the excellent mechanical property of the graphene films.

2.3. Multi-directional writing: assembly of stretchable architectures

In this section we describe multi-directional writing, very recently developed as an alternative approach, for highly conductive organic or inorganic materials onto elastic substrates.

Stretchable architectures, instead of stretchable interconnect materials that are limited to 2D structure, of 3D structural configurations have been successfully realized by two innovative approaches: (1) mechanical buckling and (2) multi-directional writing. The mechanical buckling approach, as described in section 2.1.1, led to an impressive 100% stretchability for silicon nanowire coils. However, omnidirectional and individual integration of such nanosystems remained as a challenge.

The second approach, multi-directional writing, which has been suggested to overcome the above challenge, exploits a material-contained nozzle to 'write' stretchable 3D micro- and nanostructures. This approach offers not only high stretchability but also accurately controlled shapes and positioning of each stretchable 3D structure. In this section, we describe two types of multi-directional writing methods: (1) direct ink writing for stretchable metallic microelectrodes and (2) meniscus-guided writing for stretchable organic nanowires.

2.3.1. Direct ink writing for stretchable microelectrodes. The ability to pattern functional materials in planar and 3D forms is quite important for diverse emerging applications, including electronics [61–63], optics [64–66] and tissue engineering [67, 68]. Direct ink writing, which is based on the extrusion of concentrated ink through a nozzle, as shown in figure 6(*a*), enables one to fabricate various 3D architectures without the need for expensive tooling, dies or lithographic masks [61]. Specifically an ink-deposition nozzle with a computer-controlled translation stage allows one to create 3D controlled architectures onto conformal device layouts.

Flexible and stretchable silver microelectrodes were successfully demonstrated by direct ink writing [20] in 2009. The stretchability of the microelectrodes was significantly enhanced by configuring them into 3D arch shapes. For self-supported 3D arch shapes, the rheological behaviour of silver inks was carefully controlled. Specifically, well-controlled viscoelastic response of the inks was required to flow them through the deposition nozzle and then immediately facilitate the shape retention of the deposited features while spanning the gaps in the underlying layers. As illustrated in the viscoelastic properties of a broad range of silver nanoparticle inks (figure 6(*b*)), the variation of the elastic modulus was

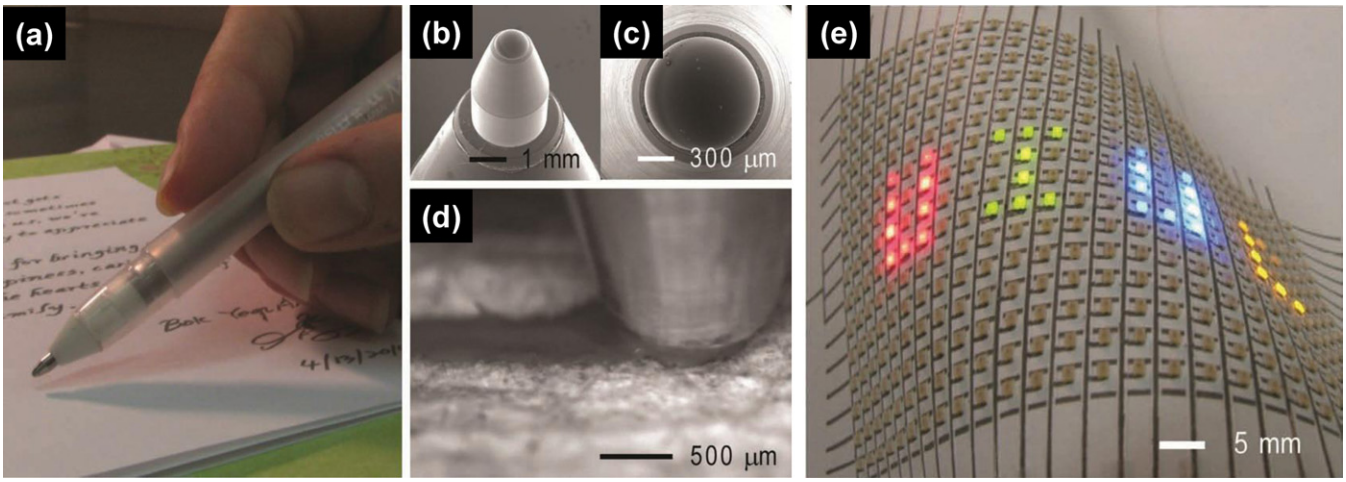

Figure 7. Pen-on-paper flexible electronics. (*a*) Optical image of a rollerball pen filled with a conductive silver ink, (*b*), (*c*) SEM images showing the rollerball pen, (*d*) optical image showing the writing process of the rollerball pen on a paper, (*e*) optical image of a flexible paper display containing an LED array interconnected by conductive silver electrodes drawn on a paper. From [69]. Reprinted with permission from Wiley.

three orders of magnitude with the nanoparticle content (60–75 wt%). A minimum elastic modulus to produce spanning features, 2000 Pa, was achieved at a silver nanoparticle concentration of ∼70 wt%.

Figure 6(*c*) shows an optical image of arched architectures that were formed by printing a spanning silver microelectrode onto a pre-strained spring and then releasing the spring. During stretching, the resistivity was maintained constant for different annealing temperatures due to its wavy shape, as seen in the plot of electrical resistivity versus strain (defined as $(L - L_0)/L_0 \times 100\%$) (figure 6(*d*)). The maximum strain of 25% was achieved at 550 °C. This result clearly showed the feasibility of 3D silver microarches for stretchable electrical interconnects.

The direct ink writing method can also be applied for integration of electrical interconnects onto flexible, paper electronics [69]. Recent attention in electronics has focused on paper substrates as a low-cost, enabling platform for flexible, lightweight and disposable devices. Importantly, the paper substrates can also be rolled or folded into 3D configuration. To realize conductive electrodes onto papers, a facile pen-on-paper approach, which is ubiquitous and portable, was successfully demonstrated. Using a rollerball pen filled with silver ink, conductive interconnects in plane and 3D platform were written. Using a rollerball pen with a ball diameter of 960 μm filled with colloidal silver ink (see figures 7(*a*)–(*c*)), a conductive line (∼650 μm in width) was printed on a paper, as shown in figure 7(*d*). A successful example of conductive electrode lines in a flexible paper is demonstrated for interconnecting LED array in figure 7(*e*). The pen-on-paper paradigm is expected to offer an effective route for printed electronic and optoelectronic devices. Its extended applications to paper-based batteries, medical diagnostics and other diverse functional devices are also anticipated using various particle-based inks such as oxide, semiconductor and carbon building blocks.

2.3.2. Meniscus-guided 3D writing of stretchable nanowires. Realization of high stretchability in nanomaterials, which is limited in the direct ink writing method, is a key challenge for future stretchable electronics. Accordingly, 3D writing, which is a promising approach to realizing stretchable devices, needs to be scaled down to nanometres for integration of stretchable nanomaterials. The meniscus-guided 3D writing method that exploits a nanoscale liquid meniscus to 'write' 3D nanostructures with designed dimensions, shapes and positioning has been developed very recently, as schematically shown in figure 8(*a*) [70]. In this method, electrodeposition or polymerization inside the nanoscale meniscus guided by pulling a micropipette enables one to fabricate metallic or polymeric 3D nanostructures.

One impressive point is that the nanowire radius r can be accurately controlled by the pulling speed v. The wire radius r is related to the pulling speed v and to W, the flow rate of the monomer solution through the pipette opening—also a function of v, by the material balance law [71]. The radius r drastically decreases as the pulling speed v increases. This is due to the balance between the flow rate of solution through the pipette opening and the growth rate of the nanowire. Figure 8(*b*) shows an example of r–v dependence of a polypyrrole nanowire grown by oxidative polymerization in air. Specifically, the radius decreased from ∼400 to ∼50 nm as the pulling speed increased from 0.5 to 1500 μm s^{-1}, using a micropipette of radius $r_0 = 0.7\,\mu$m. The importance is of course that the nanowire radius can be controlled with high accuracy by carefully tuning the pulling speed.

Remarkably a single nanowire with variable radius can be produced by changing the pulling speed during the growth. Furthermore, this approach can yield dense arrays of accurately shaped nano-objects. For example, the FE-SEM image of figure 8(*c*) shows an array of PPy nanocandles, each produced with three sequential steps. Figure 8(*d*) shows the details of a nanocandle: the stand ($r = 450$ nm) obtained with a low speed of 0.5 μm s^{-1}, the body ($r = 225$ nm) formed by abruptly increasing the speed to 12.5 μm s^{-1}, and the flame with variable radius (250–50 nm), the result of accelerating from 12.5 to 1500 μm s^{-1} for 0.01 s. Figure 8(*c*) also shows

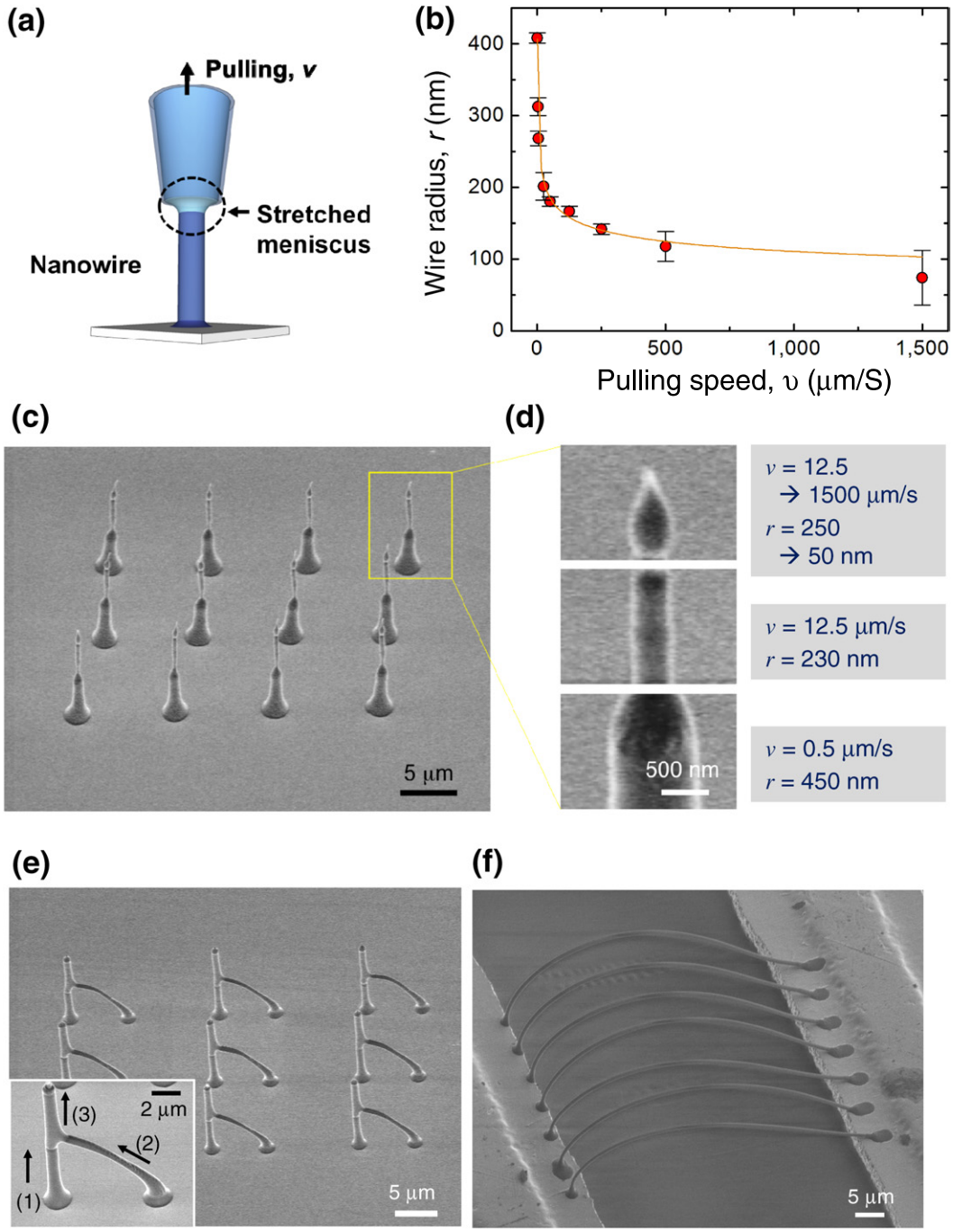

Figure 8. Fabrication of PPy nanowire. (*a*) Schematic explanation of PPy nanowire fabrication by pulling a micropipette filled with a Py monomer solution and stretching the meniscus during oxidative polymerization. (*b*) Plot of radius r versus pulling speed v for a pipette radius $r_0 = 0.7\,\mu$m. The solid line corresponds to a functional dependence $r \sim v^{-0.17}$. (*c*), (*d*) Fabrication of complex shaped PPy nanowires by tuning the pulling speed. (*c*) FE-SEM image of a specific example: an array of nanocandles (micropipette radius $r_0 = 0.7\,\mu$m). (*d*) Magnified images of the stand, body and flame of a nanocandle. (*e*), (*f*) FE-SEM images of 3D PPy nanowire arrays with different shapes and sizes and accurate individual positioning. (*e*) An array of nanobranches ($r \sim 440$ nm), each produced (inset) in three steps with different pulling directions and times ($v = 0.5\,\mu\mathrm{m\,s^{-1}}$), (*f*) an array of nanoarch bridges ($r \sim 240$ nm) between two Cu substrates separated by a ~50 μm gap. From [70]. Reprinted with permission from Wiley.

that each nanocandle in the 10 μm-step array was accurately positioned by the two-axis micropipette motion.

The technique is not only very accurate as far as size, shape and position controls are concerned, but also rather versatile. Figure 8(*e*) shows freestanding PPy nanobranches with subcomponents of controlled length and direction. Each nanobranch ($r \sim 440$ nm) was fabricated by three consecutive steps with different pulling directions (vertical, diagonal and vertical, as shown in the inset) at a speed of $0.5\,\mu\mathrm{m\,s^{-1}}$. Another interesting product is the PPy nanoarch-bridge array of figure 8(*f*). Each nanoarch ($r \sim 240$ nm) connects two Cu substrates separated by 50 μm. Nano-features of this type can be used, of course, for wafer interconnection in 3D electronics [72].

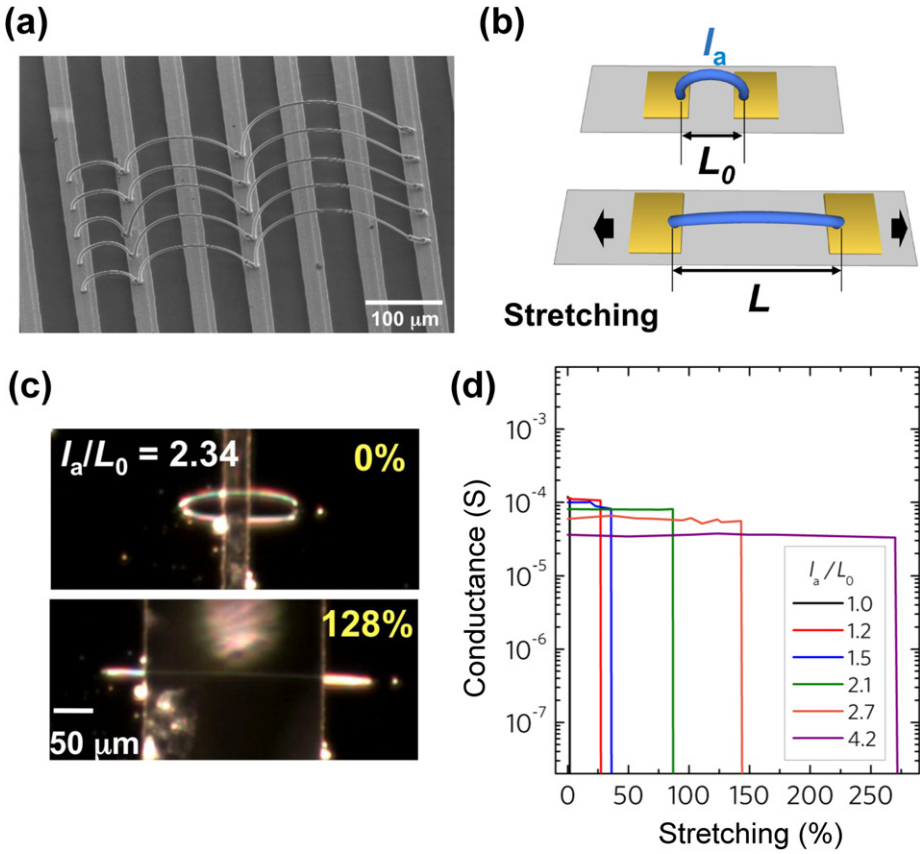

Figure 9. Stretchable microarches. (*a*) FE-SEM image of PEDOT : PSS microarch array (radius: 1.5 μm) on a Au-patterned substrate; arc length was individually controlled in the range 150–450 μm. (*b*) Scheme of stretching an arch structure between two electrodes embedded in PDMS. (*c*) Optical micrographs showing the stretching up to ≈130% of a $l_a/L_0 = 2.34$ microarch. (*d*) Conductance versus stretching for different l_a/L_0 ratios.

This approach can be applied for stretchable electronics, in particular, based on 3D micro- or nano-arches of organic conducting polymers. Accurate 3D guiding of a PEDOT : PSS meniscus by pulling a solution-filled micropipette enabled us to fabricate 3D micro- or nanowires with controlled dimensions, site-specific positioning and tunable electrical transport properties. FE-SEM image of figure 9(*a*), for example, shows an array of PEDOT : PSS freestanding wires (radius: 1.5 μm) on a Au-patterned substrate; arc length was individually controlled in the range 150–450 μm.

The key result of our study is that the microarches reached remarkable stretchability levels—defined as the stretching $(L - L_0)/L_0$ at breakage (where L and L_0 are the stretched and unstretched distances between the two feet) (figure 9(*b*)). The stretchability is expected to increase with the l_a/L_0 ratio, where l_a is the arc length: this was confirmed by measurements on ∼1 μm radius microarches grown between two Pt-coated Si wafers embedded in PDMS. The optical micrographs in figure 9(*c*) (top) show the stretching of a microarch with $l_a/L_0 = 2.3$; this specific microarch had a stretchability of ≈130%.

The plots in figure 9(*d*) show the stretching test for the microarches of a PEDOT : PSS (doped with 2.0 wt% DMSO), 1 μm radius and different l_a/L_0 ratios in the 1.0–4.2 range. The conductivity, 200 S cm^{-1}, of the microarches is independent of l_a/L_0. Most importantly, the microarch conductance

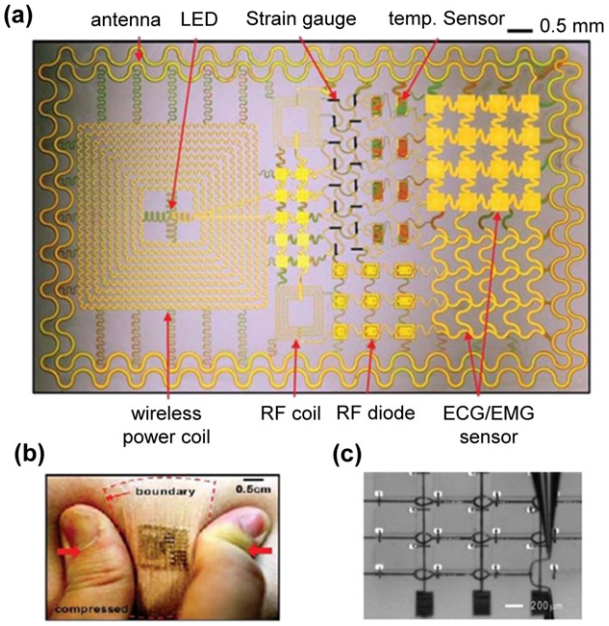

Figure 10. (*a*) Optical image of all integrated electronic devices, mounting to the skin using water soluble PVA, (*b*) multifunctional epidermal electronic system (EES) attached to skin in compressed form, (*c*) optical image acquired during patterning of silver interconnects on a gallium arsenide based, 4-by-4 LED array. From [74]. Reprinted with permission from AAAS.

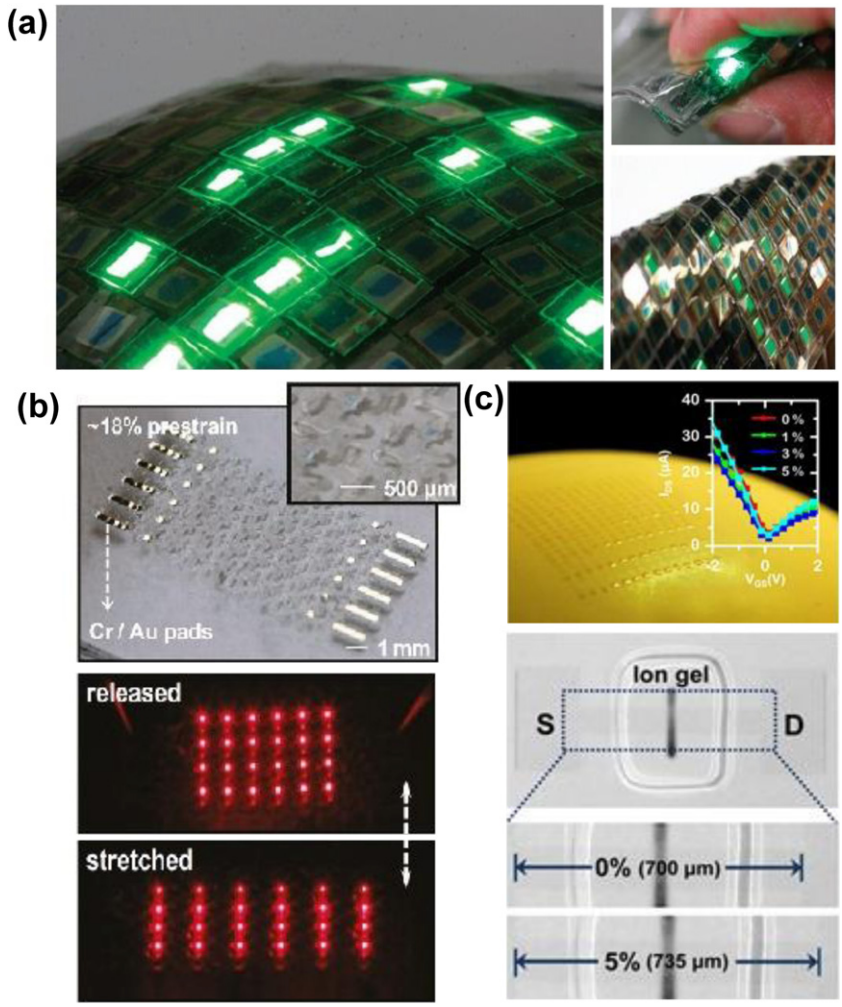

Figure 11. (*a*) Stretchable AMOLED spread over arbitrary curved surfaces (left frame). The stretchable display is functional even when folded or crumpled (right frame). Reprinted by permission from Macmillan Publishers Ltd: [7], copyright 2009. (*b*) Optical image (top) of μ-ILEDs with noncoplanar serpentine graphene interconnect bridges on a thin ($\sim$400 μm) PDMS. The inset shows a magnified view. Lower two images show the emission of light at released and stretching states, respectively. (*c*) Photograph and transfer characteristics (for 0%, 1%, 3% and 5% strain) of the ion gel-gated graphene FETs on balloon and images of tri-layer graphene FETs under 5% strain along the longitudinal direction of the channel. Reprinted with permission [76, 77]. Copyright 2011 American Chemical Society.

stays constant during stretching until foot breakage: this is of course a very interesting feature for stretchable microelectronics applications. The maximum stretchability from our measurements was 270% for $l_a/L_0 = 4.2$, a rather impressive level 50 times larger than for PEDOT : PSS films [73]. This is of course a very interesting feature for stretchable electronics applications.

3. Applications: stretchable electronics and integrated systems

We reviewed recent progressive research works, in previous sections, on developing new architectures and materials with the purpose of achieving maximum compatibility of the fabricated electronic components in terms of flexibility and stretchability. To realize flexible and stretchable electronics in the real world, one needs to demonstrate the complete devices or integrated systems. Substantial attempts have been carried out in this direction by many research groups.

Recently Kim *et al* successfully demonstrated the stretchable electronics in biomedical applications using the concept for wavy structure and 2D or 3D configuration of conventional materials discussed in section 2.1 [74]. They were able to fabricate the electrodes, sensors, power supplies, communication components and other useful electronics all together into an ultrathin, low-modulus, light weight, stretchable 'skin like' membrane that could be laminated invisibly onto skin just like transferring a temporary tattoo (figure 10(*a*)). For high-performance, well-established electronic materials of silicon and gallium arsenide in the form of nanoribbons, micro- and nanomembranes were used as active device islands. As shown in figure 10(*b*), the integrated electronic system was attached in a compressed form to the skin using thin ($\sim$50 μm) water soluble polyvinyl alcohol as temporary support. The adhesion to the skin was robust via van der Waals forces alone. The mechanical properties of the integrated system such as Young's modulus, thickness and elastic response to tensile strain were very well matched to

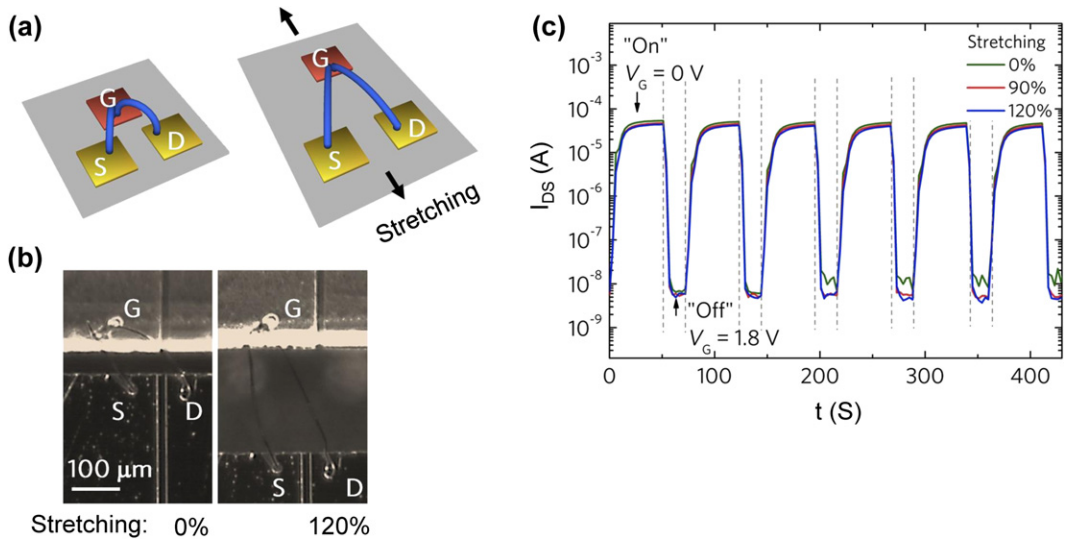

Figure 12. Highly stretchable organic electronic devices: electrochemical transistors (ECTs) with PEDOT : PSS microarches. (*a*) Unstretched and stretched ECT: S = source, G = electrolyte gate, D = drain; (*b*) optical micrographs showing an ECT stretched up to 120%, (*c*) drain–source current I_{ds} versus time during periodic 0–1.8 V switching of the gate voltage V_g for an ECT under different stretching conditions.

those of the skin. Thus the integrated electronic system was referred to as an 'epidermal electronic system' (EES).

In addition, Ahn *et al* [20] successfully demonstrated solar microcell and gallium arsenide based light-emitting diodes (4-by-4 pixels, where each pixel is 500 by 500 by 2.5 μm and spaced 200 μm apart) using direct ink writing of metal microelectrodes described in section 2.3.1 (figure 10(*c*)). The spanning silver microelectrodes were printed using an ink made of concentrated silver nanoparticles that flows through micronozzles in air.

Sekitani *et al* carried out a successful demonstration of a rubber-like stretchable active-matrix organic light-emitting diode (AMOLED) using printable elastic conductors described in earlier section 2.2.2 [75]. Each driving cell consists of a selector transistor (T) which enables the addressing of each OLED for light emission, driver transistor which control the luminescence, a capacitor (C) and printed elastic conductors. The device shows good operation of large-area OLEDs using driving cells with 2T1C structure. The left-hand side of figure 11(*a*) shows the demonstration of light-emitting display coming out from the fabricated stretchable AMOLED. Folding of AMOLED also does not cause any electrical and mechanical damage as indicated on the right-hand side of figure 11(*a*).

Nowadays, graphene is also a very promising material due to its high conductivity and excellent stretchability providing its potential use in fabrication of flexible, stretchable electronics, as described in section 2.2.3. Recent works demonstrated stretchable interconnects and transistors using these outstanding properties of graphene thin films [76, 77]. Figure 11(*b*) shows the optical image of μ-LEDs (4 × 6 arrays) interconnected by noncoplanar serpentine graphene films on PDMS substrate. These devices exhibit a uniform and constant light emission coming from the μ-LEDs at releasing and stretching states. Figure 11(*c*) presents stretchable graphene-based FETs on PDMS substrate, which can stably operate at high strain over 5%. To explore their further applicability to flexible electronics, graphene FETs were fabricated on rubber balloons. These fully stretchable electronic devices function well under large stretching. These results suggest that the graphene-based devices can robustly operate during large strain without any structural designs of device, such as wavy configurations.

The meniscus-guided writing approach described in section 2.3.2 can be used to realize stretchable electronics, including various device applications. Figures 12(*a*) and (*b*) show stretchable electrochemical transistors (ECTs) integrated using the meniscus-guided writing method [70, 78]. Their source (S), the electrolyte-coated gate (G) and the drain (D) are connected by stretchable organic microarches. The conductivity switching of transistor is controlled by a reversible redox reaction in the PEDOT : PSS in contact with the electrolyte. The transistor turns 'on' and 'off' for zero and high gate voltage, respectively. The on/off switching shows stable operation even at 90% and 120% stretching, as shown in figure 12(*c*). These procedures represent a realistic and scalable pathway to stretchable electronics.

4. Summary

This paper reviewed recent works on the materials and the architectures for high-performance stretchable electronics in two- or three-dimensional layouts.

We discussed various architectures and their integrations, ranging from wavy structural configuration and stretchable interconnects by conducting material/elastomer composites to multi-directional writing of highly conductive materials for fabricating a variety of stretchable electronic devices. These approaches could enable high-performance electronics on compliant substrates such as plastic or rubber, as demonstrated in the application examples. In particular, multi-directional writing could provide a promising route to develop future stretchable electronic applications such as robotic sensory

skins and wearable electronics that would be difficult to achieve using conventional materials and methods.

Acknowledgment

This work was supported by the Creative Research Initiatives (Functional X-ray Imaging) of MEST/NRF. J-H A acknowledges the support from the Basic Science Research Program (2011-0006268) of MEST/NSF.

References

[1] Someya T, Kato Y, Sekitani T, Lba S, Noguchi Y, Murase Y, Kawaguchi H, Sakurai T and Whitesides G M 2005 *Proc. Natl Acad. Sci. USA* **102** 12321
[2] Carta R, Jourand P, Hermans B, Thone J, Brosteaux D, Vervust T, Bossuyt F, Axisa F, Vanfleteren J and Puers R 2009 *Sensors Actuators* A **156** 79–87
[3] Kim D H, Ahn J H, Choi W M, Kim H S, Kim T H, Song J, Huang Y Y, Liu Z, Lu C and Rogers J A 2008 *Science* **320** 507
[4] Rogers J A and Huang Y 2009 *Proc. Natl Acad. Sci. USA* **106** 10875
[5] Rogers J A, Someya T and Huang Y 2010 *Science* **327** 1603
[6] Brosteaux D, Axisa F, Gonzalez M and Vanfleteren J 2007 *IEEE Electron Device Lett.* **28** 552
[7] Kim D H, Song J, Choi W M, Kim H S, Kim R H, Liu Z, Huang Y Y, Hwang K C, Zhang Y W and Rogers J A 2008 *Proc. Natl Acad. Sci. USA* **105** 18675
[8] Lacour S P, Jones J, Wagner S, Li T and Suo Z 2005 *Proc. IEEE* **93** 1459
[9] Siegel A C, Bruzewicz D A, Weibel D B and Whitesides G M 2007 *Adv. Mater.* **19** 727
[10] Hansen T S, West K, Hassager O and Larsen N B 2007 *Adv. Funct. Mater.* **17** 3069
[11] Sekitani T, Noguchi Y, Hata K, Fukushima T, Aida T and Someya T 2008 *Science* **321** 1468
[12] Chun K Y, Oh Y, Rho J, Ahn J H, Kim Y J, Choi H R and Baik S 2010 *Nature Nanotechnol.* **5** 853
[13] Kim K S, Zhao Y, Jang H, Lee S Y, Kim J M, Kim K S, Ahn J H, Kim P, Choi J Y and Hong B H 2009 *Nature* **457** 706
[14] Jones J, Lacour S P, Wagner S and Suo Z 2004 *J. Vac. Sci. Technol.* A **22** 1723
[15] Adrega and Lacour S P 2010 *J. Micromech. Microeng.* **20** 055025
[16] Ishikawa F N, Chang H K, Ryu K, Chen P C, Badmaev A, De Arco L G, Shen G and Zhou C 2009 *ACS Nano* **3** 73
[17] Wiedeman S, Wendt R G and Britt J S 1999 *AIP Conf. Proc.* **462** 17
[18] Loher T, Seckel M, Vieroth R, Dils C, Kallmayer C, Ostmann A, Aschenbrenner R and Reichl H 2009 *IEEE 11th Electronics Packing Technology Conf.* p 893
[19] Hosokawa M, Nogi K, Naito M and Yokoyama T 2007 *Nanoparticle Technology Handbook* 1st edn (Oxford: Elsevier)
[20] Ahn B Y, Duoss E B, Motola M J, Guo X, Park S-II, Xiong Y, Yoon J, Nuzzo R G, Rogers J A and Lewis J A 2009 *Science* **323** 1590
[21] Khang D Y, Jiang H, Huang Y and Rogers J A 2006 *Science* **311** 208–12
[22] Ko H C *et al* 2008 *Nature* **454** 748–53
[23] Qi Y, Kim J, Nguyen T D, Lisko B, Purohit P K and McAlpine M C 2011 *Nano Lett.* **11** 1331–6
[24] Sun Y, Choi W M, Jiang H, Huang Y Y and Rogers J A 2006 *Nature Nanotechnol.* **1** 201–7
[25] Ryu S Y, Xiao J, Park W I, Son K S, Huang Y Y, Paik U and Rogers J A 2009 *Nano Lett.* **9** 3214–9
[26] Khang D-Y, Xiao J, Kocabas C, MacLaren S, Banks T, Jiang H, Huang Y Y and Rogers J A 2008 *Nano Lett.* **8** 124–30
[27] Xiao J, Carlson A, Liu Z J, Huang Y, Jiang H and Rogers J A 2008 *Appl. Phys. Lett.* **93** 013109
[28] Axisa F, Brosteaux D, De Leersnyder E, Bossuyt F, Vanfleteren J, Hermans B and Puers R 2007 *Proc. IEEE-EMBS (2007)* pp 5687–90
[29] Gray D S, Tien J and Chen C S 2004 High-conductivity elastomeric electronics *Adv. Mater.* **16** 393–7
[30] Huyghe B and Rogier H 2008 *IEEE Trans. Adv. Packag.* **31** 802
[31] Gonzalez M, Axisa F, Vanden Bulcke M, Brosteaux D, Vandevelde B and Vanfleteren J 2008 *Microelectron. Reliab.* **48** 825
[32] Brosteaux D, Axisa F, Gonzalez M and Vanfleteren J 2007 *IEEE Electron Device Lett.* **28** 552–4
[33] Jackman R J, Brittain S T, Adams A, Prentiss M G and Whitesides G M 1998 *Science* **280** 2089
[34] Brittain S T, Schueller O J A, Wu H K, Whitesides S and Whitesides G M 2001 *J. Phys. Chem.* B **105** 347
[35] LaVan D A, George P M and Langer R 2003 *Angew. Chem. Int. Edn* **42** 1262
[36] Lee H K, Chang S I and Yoon E 2006 *J. Microelectromech. Syst.* **15** 1681
[37] Piotter V, Benzler T, Gietzelt T, Ruprecht R and Hausselt J 2000 *Adv. Eng. Mater.* **2** 639
[38] Chung S, Park S, Lee I, Jeong H and Cho D 2005 *Microsyst. Technol.* **11** 424
[39] Lea C 1988 *A Scientific Guide to Surface Mount Technology* (Ayr: Electrochemical Publications)
[40] Hwang J S 1996 *Modern Solder Technology for Competitive Electronics Manufacturing* (Boston, MA: McGraw-Hill)
[41] Siegel A C, Bruzewicz D A, Weibel D B and Whitesides G M 2007 *Adv. Mater.* **19** 727–33
[42] Kim D H and Rogers J A 2009 *ACS Nano* **3** 498–501
[43] Xie J, Pecht M, DeDonato D and Hassanzadeh A 2001 *Microelectron. Reliab.* **21** 281
[44] Tamai T 1982 *IEEE Trans. Compon. Hybrids Manuf. Technol.* **5** 56
[45] Wha Oh K, Park H J and Kim S H 2003 *J. Appl. Polym. Sci.* **88** 1225
[46] Heisey C L, Wightman J P, Pittman E H and Kuhn H H 2005 *Sensors Actuators* B **109** 329
[47] Oh K W, Hong K H and Kim S H 1999 *J. Appl. Polym. Sci.* **74** 2094
[48] Shenoy S L, Cohen D, Erkey C and Weiss R A 2002 *Indust. Eng. Chem. Res.* **41** 1484
[49] He F F, Omoto M, Yamamoto T and Kise H 1995 *J. Appl. Polym. Sci.* **55** 283
[50] Fu Y P, Weiss R A, Gan P P and Bessette M D 1998 *Polym. Eng. Sci.* **38** 857
[51] Hansen T S, West K, Hassager O and Larsen N B 2007 *Adv. Funct. Mater.* **17** 3069–73
[52] Kato Y, Sekitani T, Takamiya M, Doi M, Asaka K, Sakurai T and Someya T 2007 *IEEE Electron Device Lett.* **54** 202
[53] Sekitani T, Noguchi Y, Hata K, Fukushima T, Aida T and Someya T 2008 *Science* **321** 1468
[54] Chun K-Y, Oh Y, Rho J, Ahn J-H, Kim Y-J, Choi H R and Baik S 2010 *Nature Nanotechnol.* **5** 853
[55] Yang D-Q, Hennequin B and Sacher E 2006 *Chem. Mater.* **18** 5033–8
[56] Yang G-W *et al* 2008 *Carbon* **46** 747–52
[57] Oh Y, Suh D, Kim Y-J, Han C-S and Baik S 2011 *J. Nanosci. Nanotech.* **11** 489
[58] Oh Y, Chun K-Y, Lee E, Kim Y-J and Baik S 2010 Nano-silver particles assembled on one-dimensional nanotube scaffolds

for highly conductive printable silver/epoxy composites *J. Mater. Chem.* **20** 3579–82
[59] Bae S *et al* 2010 *Nature Nanotechnol.* **5** 574
[60] Lee C, Wei X, Kysar J W and Hone J 2008 *Science* **321** 385
[61] Lewis J A and Gratson G M 2004 *Mater. Today* 32–9
[62] Ahn B Y, Lorang D J, Duoss E B and Lewis J A 2010 *Chem. Commun.* **46** 7118–20
[63] Adams J J, Duoss E B, Malkowsji T F, Motala M J, Ahn B Y, Nuzzo R G, Bernhard J T and Lewis J A 2011 *Adv. Mater.* **23** 1335–40
[64] Parker S T, Domachuk P, Amsden J, Bressner J, Lewis J A, Kaplan D L and Omenetto F G 2009 *Adv. Mater.* **21** 2411–5
[65] Arpin K A, Mihi A, Johnson H T, Bacam A J, Rogers J A, Lewis J A and Braun P V 2010 *Adv. Mater.* **22** 1084–101
[66] Lorang D J, Tanaka D, Spadaccini C M, Rose K A, Cherepy N J and Lewis J A 2011 *Adv. Mater.* **23** 5055–8
[67] Hanson Shepherd J N, Parker S T, Shepherd R F, Gillette M U, Lewis J A and Nuzzo R G 2011 *Adv. Funct. Mater.* **21** 47–54
[68] Barry R A III, Shepherd R F, Hanson J N, Nuzzo R G, Wiltzius P and Lewis J A 2009 *Adv. Mater.* **21** 1–4
[69] Russo A, Ahn B Y, Adams J J, Duoss E B, Bernhard J T and Lewis J A 2011 *Adv. Mater.* **23** 3426–30
[70] Kim J T, Seol S K, Pyo J, Lee J S, Je J H and Margaritondo G 2011 *Adv. Mater.* **23** 1968
[71] Gou Z and McHugh A J 2004 *J. Non-Newtonian Fluid Mech.* **118** 121
[72] Hu J and Yu M-F 2010 *Science* **329** 313
[73] Lang U and Dual J 2007 *Key Eng. Mater.* **345** 1189
[74] Kim D-H *et al* 2011 *Science* **333** 838
[75] Sekitani T, Nakajima H, Maeda H, Fukushima T, Aida T, Hata K and Someya T 2009 *Nature Mater.* **8** 494
[76] Kim R-H *et al* 2011 *Nano Lett.* **11** 3881–6
[77] Lee S-K *et al* 2011 *Nano Lett.* **11** 4642–6
[78] Kim J T, Pyo J, Rho J, Ahn J-H, Je J H and Margaritondo G 2012 *ACS Macro Letters*, http://dx.doi.org/10.1021/mz200249c